

## **Characterization of submicron organic particles in Beijing during summertime: Comparison between SP-AMS and HR-AMS**

Junfeng Wang<sup>1,2</sup>, Jianhuai Ye<sup>2</sup>, Dantong Liu<sup>3</sup>, Yangzhou Wu<sup>3</sup>, Jian Zhao<sup>4</sup>, Weiqi Xu<sup>4</sup>,  
Conghui Xie<sup>4</sup>, Fuzhen Shen<sup>1</sup>, Jie Zhang<sup>5</sup>, Paul E. Ohno<sup>2</sup>, Yiming Qin<sup>2</sup>, Xiuyong Zhao<sup>6</sup>,  
Scot T. Martin<sup>2</sup>, Alex K.Y. Lee<sup>7</sup>, Pingqing Fu<sup>8</sup>, Daniel J. Jacob<sup>2</sup>, Qi Zhang<sup>9</sup>, Yele Sun<sup>4</sup>,  
Mindong Chen<sup>1</sup> and Xinlei Ge<sup>1,\*</sup>

<sup>1</sup>Jiangsu Key Laboratory of Atmospheric Environment Monitoring and Pollution Control, Collaborative Innovation Center of Atmospheric Environment and Equipment Technology, School of Environmental Science and Engineering, Nanjing University of Information Science and Technology, Nanjing, China

<sup>2</sup>School of Engineering and Applied Sciences, Harvard University, Cambridge, MA, United States

<sup>3</sup>Department of Atmospheric Sciences, School of Earth Sciences, Zhejiang University, Hangzhou, China

<sup>4</sup>State Key Laboratory of Atmospheric Boundary Layer Physics and Atmospheric Chemistry, Institute of Atmospheric Physics, Chinese Academy of Sciences, Beijing, China

<sup>5</sup>Department of Atmospheric Science, Colorado State University, Fort Collins, CO, United States

<sup>6</sup>State Environmental Protection Key Laboratory of Atmospheric Physical Modeling and Pollution Control, State Power Environmental Protection Research Institute, Nanjing, China

<sup>7</sup>Department of Civil and Environmental Engineering, National University of Singapore, Singapore

<sup>8</sup>Institute of Surface-Earth System Science, Tianjin University, Tianjin, China

<sup>9</sup>Department of Environmental Toxicology, University of California Davis, Davis, CA, United States

\*Corresponding author: Xinlei Ge (Email: caxinra@163.com)

1 **ABSTRACT**

2 Black carbon (BC) particles in Beijing summer haze play an important role in  
3 regional radiation balance and related environmental processes. Understanding the  
4 factors that lead to variability of the impacts of BC remains limited. Here, we present  
5 observations by a soot-particle aerosol mass spectrometer of BC-containing submicron  
6 particulate matter (BC-PM<sub>1</sub>) in Beijing, China during 2017 summer. These observations  
7 were compared to concurrently measured total non-refractory submicron particulate  
8 matter (NR-PM<sub>1</sub>) by a high-resolution aerosol mass spectrometer (HR-AMS). Distinct  
9 properties were observed between NR-PM<sub>1</sub> and BC-PM<sub>1</sub> relevant to organic aerosol  
10 (OA) composition. Hydrocarbon-like OA in BC-PM<sub>1</sub> was found to be up to two-fold  
11 higher than that in NR-PM<sub>1</sub> in fresh vehicle emissions, suggesting that a part of HOA  
12 in BC-PM<sub>1</sub> may be overestimated, likely due to the change of collection efficiency of  
13 SP-AMS. Cooking-related OA was only identified in NR-PM<sub>1</sub>, whereas aged biomass  
14 burning OA (A-BBOA) was a unique factor only identified in BC-PM<sub>1</sub>. The A-BBOA  
15 was linked to those heavily coated BC, which may lead to enhancement of light  
16 absorption ability of BC by a factor of two via the “lensing effect”. More-oxidized  
17 oxygenated OA identified in BC-containing particles was found to be slightly different  
18 from that observed by HR-AMS, mainly due to the influence of A-BBOA. Overall,  
19 these findings highlight that BC in urban Beijing is partially of agricultural fire origin  
20 and, a unique biomass burning-related OA associated with BC may be ubiquitous in  
21 aged BC-PM<sub>1</sub>, and this OA may play a role in affecting air quality and climate that has  
22 not previously been fully considered.

## 23 **1. Introduction**

24 Black carbon (BC) is an important component of atmospheric aerosol that exerts  
25 negative effects on regional radiation balance (Bond et al., 2013) and human health  
26 (Janssen, 2012). It absorbs solar radiation, leading to direct atmospheric heating  
27 (Ramanathan and Carmichael, 2008). Indirectly, BC-containing particles (BCc) can  
28 also serve as cloud condensation nuclei upon mixing with hydrophilic species (e.g.,  
29 sulfate), resulting in changes in cloud properties (Wu et al., 2019). Inhalation of BC is  
30 associated with adverse health impacts such as respiratory diseases and birth defects  
31 (Janssen, 2012).

32 BC particles are released to the atmosphere directly and usually mixed with non-  
33 BC materials (e.g., inorganic and organic) from incomplete fuel combustion and open  
34 fires (Ramanathan and Carmichael, 2008; Bond et al., 2013; Chen et al., 2013). Non-BC  
35 species also can coat onto primary BCc in the atmosphere through condensation and/or  
36 coagulation processes (Lee et al., 2017). These atmospheric processes gradually alter  
37 the mixing state and the morphology (e.g., from an externally-mixed fractal structure  
38 (Buseck et al., 2014) into an internally-mixed “core-shell” structure (China et al., 2015))  
39 of BCc. These alterations can enhance the light absorption capacity of the BC core via  
40 the “lensing effect” due to the increased light absorption cross-section as a result of the  
41 enhanced coating thickness (Saleh et al., 2015; Cappa et al., 2012). Additionally, the  
42 chemical constituents of BCc may dynamically change during the aging processes,  
43 which also lead to changes in the light absorption capacity of the particles (Wang et al.,  
44 2019; Wang et al., 2017). Because these physical and chemical processes of both  
45 organic and inorganic species inside BCc continuously alter particle properties  
46 throughout the lifetime of the particles, great uncertainty remains in quantifying the  
47 light absorption ability of BC (Liu et al., 2018; Liu et al., 2019). Understanding the  
48 relationship of mixing state and chemical composition to the light absorption properties  
49 of BCc, as well as its spatiotemporal distribution, is of importance to accurately  
50 evaluate the impacts of BC in regional air quality.

51 Aerodyne high-resolution aerosol mass spectrometry (HR-AMS) (Canagaratna et  
52 al., 2007) has been widely applied in field studies to investigate the chemically-resolved

53 composition of non-refractory submicron particulate matter (NR-PM<sub>1</sub>, species that  
54 vaporize at temperature < 600 °C)(Li et al., 2015;Lee et al., 2013;Sun et al., 2012;Ge  
55 et al., 2012b;Ge et al., 2012a;Xu et al., 2019b;Sun et al., 2014). However, the working  
56 temperature of the standard HR-AMS tungsten vaporizer (600 °C) is not sufficient to  
57 vaporize refractory species such as BC. To overcome this limitation, soot-particle  
58 aerosol mass spectrometry (SP-AMS) is developed (Onasch et al., 2012). In addition to  
59 the standard tungsten vaporizer, SP-AMS is equipped with a laser vaporizer (with a  
60 wavelength of 1064 nm) which selectively heats BC (core), together with the non-BC  
61 species mixed with it (Wang et al., 2016). This novel technique makes it possible to  
62 compare the compositions of submicron BCc (BC-PM<sub>1</sub>) and NR-PM<sub>1</sub>, allowing a more  
63 accurate assessment of the impacts of BC. However, a question is whether the ion  
64 fragments of organic species ionized by the 70eV electron impact of SP-AMS and HR-  
65 AMS are the same in terms of different thermal schemes. It has been reported that the  
66 mass spectra of NR-PM<sub>1</sub> organic have high m/z 44 (mainly CO<sub>2</sub><sup>+</sup>) signal, while the  
67 mass spectra of BC-related organics have high m/z 43 (C<sub>3</sub>H<sub>7</sub><sup>+</sup> and C<sub>2</sub>H<sub>3</sub>O<sup>+</sup>) signal. The  
68 reason for this is the SP-AMS provides vaporization of the BC-PM<sub>1</sub> at lower  
69 temperatures compared to the standard tungsten vaporizer of the HR-AMS, resulting in  
70 less overall fragmentation and therefore less CO<sub>2</sub><sup>+</sup> production in the laser, in addition,  
71 the lower fragmentation also causes the presence of more ion fragments at m/z > 100  
72 amu in the SP-AMS mass spectra compared to that of HR-AMS (Canagaratna et al.,  
73 2015b;Massoli et al., 2015). Nevertheless, quantification of BC-PM<sub>1</sub> organic aerosol  
74 (OA) factors identified from positive matrix factorization (PMF) has been reported that  
75 were not significantly affected by the differences of mass spectra between HR-AMS  
76 and SP-AMS (Lee et al., 2017;Massoli et al., 2015).

77 To date, there have only been a few studies that have compared the differences of  
78 species in BC-PM<sub>1</sub> and NR-PM<sub>1</sub> (Lee et al., 2017;Collier et al., 2015;Massoli et al.,  
79 2015). Lee et al. found that cooking-related organic aerosol (COA) may externally mix  
80 with BC in summertime California (Lee et al., 2017). The COA factor was identified in  
81 NR-PM<sub>1</sub> organic aerosol (OA), but not in the BC-related OA. Wang et al found that  
82 transported biomass burning organic aerosol could be thickly coated on BC in central

83 Tibetan Plateau and significantly enhance the light absorption capacity of BC cores  
84 (Wang et al., 2017). Interestingly, the transported biomass burning organic aerosol was  
85 not resolved in NR-PM<sub>1</sub> OA particles from concurrent HR-AMS measurements (Xu et  
86 al., 2018). These studies suggest that BC-related OA may undergo different  
87 atmospheric processes compared to those do not contain BC.

88 Beijing is a megacity known for high particulate matter (PM) concentrations. BC-  
89 PM<sub>1</sub> during haze events of summertime Beijing may have distinct sources and  
90 properties than other locations in the world. As a part of the UK-China Air Pollution  
91 and Human Health (APHH) project summer campaign (Shi et al., 2019; Chen et al.,  
92 2020a; Chen et al., 2020b), in this study, we focus on the differences of individual  
93 species between BC-PM<sub>1</sub> and NR-PM<sub>1</sub> regarding their chemical composition, mass  
94 loadings, sources, and formation pathways in summertime in urban Beijing. Results  
95 from this study provide a better understanding of the formation mechanism of OA  
96 particles in Beijing haze and valuable insights in assessing their impacts on air quality.

97

## 98 **2. Experiments**

### 99 **2.1. Sampling site and period**

100 The observations were conducted at a rooftop laboratory (8 m above ground level)  
101 in the Tower Division of the Institute of Atmospheric Physics (IAP), Chinese Academy  
102 of Sciences (CAS) in urban Beijing (39°58'N, 116°22'E), China, from 4 to 29 June,  
103 2017. This site has been reported multiple times to be a typical urban observation  
104 location (Xie et al., 2019b; Liu et al., 2019; Wang et al., 2019; Qiu et al., 2019; Xu et al.,  
105 2019a; Xie et al., 2019a). The site is located around the North 3<sup>rd</sup> Ring Road of Beijing.  
106 A highway is approximately 360 m to the east and a lot of restaurants (e.g., Sichuan  
107 style and BBQ) are within 100 m on the north side.

108

### 109 **2.2. Instrumentation**

110 Two Aerodyne Aerosol Mass Spectrometers (AMS), including a laser-only Soot-  
111 Particle AMS (SP-AMS) and a High-Resolution Time of Flight AMS (HR-AMS) were  
112 deployed to measure chemical compositions and size distributions of BC-PM<sub>1</sub> and NR-

113 PM<sub>1</sub>, respectively. Three types of species were measured during the campaign: NR-  
114 PM<sub>1</sub>, including non-refractory species that don't mix with BC (Type I) and non-  
115 refractory species that mixed with BC (Type II), and BC-PM<sub>1</sub> (BC core and both  
116 refractory and non-refractory species coated on the core)(Type III). NR-PM<sub>1</sub> can be  
117 quickly vaporized by the 600 °C tungsten vaporizer of HR-AMS and be detected. The  
118 SP-AMS used here was equipped only with the Nd-YAG intra-cavity infrared laser  
119 (1064 nm) (tungsten vaporizer was physically removed), it can selectively detect BC-  
120 containing particles only, which include Type II and Type III species. A shared PM<sub>2.5</sub>  
121 cyclone inlet (Model URG-2000-30ED) with 3 Lpm flowrate and a diffusion dryer were  
122 used prior to the sampling. The detailed information on the operation of HR-AMS and  
123 SP-AMS during the sampling campaign can be found in previous literature (Xie et al.,  
124 2019a; Xu et al., 2019b). Details of tuning, calibration, and configurations of the two  
125 AMS instruments can be seen in our previous papers (Wang et al., 2019; Xu et al.,  
126 2019a; Xu et al., 2019b). The two AMS were operated under the V-mode which is  
127 favorable for mass quantification with a time resolution of five minutes. Mixing ratios  
128 of O<sub>3</sub>, and NO<sub>2</sub> (Thermo Fisher Scientific, model 49i and model 42C) were measured  
129 in parallel simultaneously. Vertical meteorological parameters, including temperature  
130 (*T*) and relative humidity (*RH*), were measured from the IAP 325m meteorological  
131 tower.

132

### 133 2.3. Data Analysis

134 AMS data analysis was performed by using Squirrel 1.57 and Pika 1.16I based on  
135 Igor Pro 6.37 (WaveMetrics Corp.). The measurement of filtered air was performed for  
136 24 hours before the start of the campaign to determine the detection limits of various  
137 aerosol species and to adjust the fragmentation table. The relative ionization efficiency  
138 (RIE) of BC was calibrated with Regal Black (RB, REGAL 400R pigment black, Cabot  
139 Corp.). The average ratio of C<sub>1</sub><sup>+</sup> to C<sub>3</sub><sup>+</sup> ionized from pure BC (RB) was determined to  
140 be 0.53, which minimizes the influence of C<sub>1</sub><sup>+</sup> from non-refractory organics. The RIE  
141 of BC was determined to be 0.17 based on calibrations performed before, in the middle,  
142 and at the end of the campaign. RIEs of NO<sub>3</sub><sup>-</sup>, SO<sub>4</sub><sup>2-</sup>, NH<sub>4</sub><sup>+</sup> were determined to be 1.1,

143 0.82, and 3.82, respectively, and default values of 1.3 and 1.4 for RIEs of Chl and Org  
144 were applied, respectively (Canagaratna et al., 2007). Consistent with BC-PM<sub>1</sub>  
145 measurements in previous studies, the RIEs calibration of NO<sub>3</sub><sup>-</sup>, SO<sub>4</sub><sup>2-</sup>, NH<sub>4</sub><sup>+</sup> were  
146 performed before the tungsten vaporizer was removed, by assuming those RIEs remain  
147 unchanged throughout the campaign (Wang et al., 2017). Polystyrene latex (PSL)  
148 spheres (100-700 nm) (Duke Scientific Corp., Palo Alto, CA) were used to calibrate the  
149 particle size distribution before the campaign. The collection efficiency (CE) of 0.5  
150 were applied for both HR-AMS and SP-AMS in this study. It should be noted that, the  
151 BC quantification will not be affected by particle bouncing without the tungsten  
152 vaporizer, which could affect the CE in the standard HR-AMS measurements  
153 (Canagaratna et al., 2007). However, the CE will be governed by the overlap of particle  
154 beam and laser beam (Lee et al., 2017; Massoli et al., 2015; Willis et al., 2014). Both  
155 HR-AMS and SP-AMS resolved mass concentrations of NR-PM<sub>1</sub> and BC were  
156 calculated based on V-mode high-resolution fitting. Due to different vaporization  
157 schemes between the HR-AMS and SP-AMS, mass spectra from these two instruments  
158 even for the same population of aerosols are not entirely the same. Because laser-only  
159 SP-AMS generally results in less overall fragmentation, its mass profile may contain  
160 more large *m/z* fragments and less small *m/z* fragments compared to that from HR-  
161 AMS (Massoli et al., 2015). In addition, the elemental ratios of organics reported here,  
162 i.e., oxygen-to-carbon and hydrogen-to-carbon ratios (O/C and H/C) were calculated  
163 based on the “Improved-Ambient (I-A)” method (Canagaratna et al., 2015a) (scaling  
164 factors of 1.10 for H:C and 0.86 for O:C were applied for elemental ratios calculated  
165 from SP-AMS data)

166 Positive matrix factorization (PMF) (Paatero and Tapper, 1994) was performed on  
167 the high-resolution organic mass spectra matrix of both NR-PM<sub>1</sub> and BC-PM<sub>1</sub> (e.g., BC  
168 (C<sub>x</sub><sup>+</sup>), and species associated with BC) across *m/z* 12–120 using PMF Evaluation Tool  
169 written in Igor (Ulbrich et al., 2009), following the standard procedure (Zhang et al.,  
170 2011). Four types of organic aerosol (OA) from total NR-PM<sub>1</sub> (see our previous  
171 paper) (Xu et al., 2019b) and five OA factors from BC-PM<sub>1</sub> were identified. C<sub>x</sub><sup>+</sup> was  
172 involved in the calculation of elemental ratios (e.g., O/C and H/C) of PMF OA factors.

173 All data presented in this paper were averaged hourly and are presented at local time  
174 (Beijing Time, UTC+8).

175

### 176 **3. Results and discussion**

#### 177 **3.1. Overview of observations**

178 Figure 1 shows the temporal variations of selected chemical species during the  
179 campaign. Information for other variables is provided in the supplementary materials  
180 (SM). The two cases labeled in Figure 1 are of interest. Case I (June 8-13) was  
181 characterized with high NO<sub>2</sub> concentrations (average  $26.7 \pm 13.5$  ppb, Table S1) and  
182 relatively low O<sub>3</sub> concentrations ( $41.7 \pm 30.0$  ppb) with NO<sub>2</sub>-to-O<sub>3</sub> ratio of 0.64. Case  
183 II (June 17-22) was featured by low NO<sub>2</sub> ( $14.9 \pm 5.9$  ppb) and high O<sub>3</sub> ( $84.6 \pm 30.6$  ppb)  
184 concentrations with an NO<sub>2</sub>-to-O<sub>3</sub> ratio of 0.18. Unlike winter Beijing haze pollution,  
185 *RH* remained at a relatively low level ( $36.5 \pm 15.3\%$ ), which is not expected to play a  
186 significant role in OA formation during the campaign (Figure 1b and Figure S1). In  
187 contrast, a strong correlation has been observed between temperature and O<sub>3</sub> ( $r^2 = 0.53$ ).  
188 The temperature was higher on average in Case II ( $29.8 \pm 3.8$  °C) than in Case I ( $26.1$   
189  $\pm 4.1$  °C).

190 The mass concentrations and mass concentration ratios of organic (Org), sulfate  
191 (SO<sub>4</sub><sup>2-</sup>) and nitrate (NO<sub>3</sub><sup>-</sup>) in NR-PM<sub>1</sub> (in solid line) and BC-PM<sub>1</sub> (in dotted line) are  
192 shown in Figures 1c-e. High correlations were observed between BC-PM<sub>1</sub> and NR-PM<sub>1</sub>  
193 measurements for SO<sub>4</sub><sup>2-</sup> ( $r^2 = 0.70$ ) and NO<sub>3</sub><sup>-</sup> ( $r^2 = 0.86$ ), but not for Org ( $r^2 = 0.49$ ).  
194 This result suggests that, BC-PM<sub>1</sub> Org has distinct sources or formation pathways from  
195 NR-PM<sub>1</sub> Org. Comparing two cases, the average mass ratios of BC-PM<sub>1</sub> to NR-PM<sub>1</sub> for  
196 SO<sub>4</sub><sup>2-</sup> and NO<sub>3</sub><sup>-</sup> in Case I ( $0.24 \pm 0.11$  and  $0.37 \pm 0.12$ ) were close to those in Case II  
197 ( $0.19 \pm 0.06$  and  $0.31 \pm 0.07$ ). However, ratios of BC-PM<sub>1</sub> to NR-PM<sub>1</sub> for Org were a  
198 factor of greater for Case I ( $0.74 \pm 0.32$ ) compare to Case II ( $0.46 \pm 0.13$ ). During the  
199 nighttime, this ratio increases to almost unity in Case I. Additionally, BC concentration  
200 in Case I (average  $2.6 \pm 1.6$  μg m<sup>-3</sup>) was 1.5 folds higher than in Case II (average  $1.7 \pm$   
201  $0.8$  μg m<sup>-3</sup>). The implication is that the organic is mostly associated with BC and likely  
202 comprised of freshly emitted compounds in Case I. This is also evident by the moderate



203 correlation between  $\text{NO}_2$  and BC-PM<sub>1</sub> Org ( $r^2 = 0.42$ ) in Case I. On the other hand, the  
204 lower Org ratio in Case II with higher  $\text{O}_3$  concentrations indicates greater oxidation and  
205 secondary processes in non-BC particles.

206

### 207 3.2. Source apportionment of BC-PM<sub>1</sub> OA

208 To further investigate the differences between organics in NR-PM<sub>1</sub> and BC-PM<sub>1</sub>,  
209 the comparison of PMF OA factors between NR-PM<sub>1</sub> and BC-PM<sub>1</sub> Org is necessary.  
210 Four factors were identified from PMF analysis of the NR-PM<sub>1</sub> Org matrix, including  
211 hydrocarbon-related OA (HOA), cooking OA (COA), less-oxidized oxygenated OA  
212 (LO-OOA), and more-oxidized oxygenated OA (MO-OOA). Details of the NR-PM<sub>1</sub>  
213 PMF analysis can be found in our previous study (Xu et al., 2019b). Here we only  
214 present the PMF results of the SP-AMS measured BC-PM<sub>1</sub> Org. As shown in Figure 2,  
215 five factors were resolved by PMF with factors including a HOA, a less oxidized OOA  
216 (OOA1), three more-oxidized OOA factors were recombined into one OOA factor  
217 (MO-OOA = Aged- biomass burning organic aerosol (A-BBOA) + OOA2 + OOA3).  
218 Diagnostic plots of this PMF solution is presented in Figure S2.

219 HOA consists of a series of hydrocarbon fragments ( $\text{C}_x\text{H}_y^+$ ) in its mass spectrum  
220 (Figure 2f), thus having a low O/C ratio (0.13) but a high H/C ratio (1.62). It has a  $r^2$  of  
221 0.92 with  $\text{C}_4\text{H}_9^+$  ( $m/z = 57$ ) and a  $r^2$  of 0.57 with  $\text{NO}_x$  (Figure 2a), indicative of its  
222 sources from vehicle emissions (Xu et al., 2019a). It also correlated tightly with BC ( $r^2$   
223 of 0.70) and a series of polycyclic aromatic hydrocarbons (PAHs) ions, e.g.,  $\text{C}_9\text{H}_7^+$  ( $m/z$   
224 115,  $r^2$  of 0.63).

225 The second factor has a remarkably high fraction of the biomass burning organic  
226 aerosol (BBOA) marker ions of  $\text{C}_2\text{H}_4\text{O}_2^+$  ( $m/z = 60$ ) (1.31%) and  $\text{C}_3\text{H}_5\text{O}_2^+$  ( $m/z = 73$ )  
227 (1.34%) in its mass spectrum (Figure 2g), much higher than that observed in non-BBOA  
228 (e.g., 0.3% at  $m/z = 60$ ) in previous studies (Sun et al., 2016; Xu et al., 2019a; Wang et  
229 al., 2017). As expected, the temporal variation of this factor correlated tightly with those  
230 of  $\text{C}_2\text{H}_4\text{O}_2^+$  and  $\text{C}_3\text{H}_5\text{O}_2^+$  ( $r^2$  of 0.71 and 0.72, respectively). In addition, the mass  
231 spectrum of this factor is strikingly similar to that of the transported BBOA which was  
232 observed at a remote site in the central Tibetan Plateau (Wang et al., 2017), with a  $r^2$  of

233 0.97. Here we categorized the transported BBOA as aged-BBOA (A-BBOA) identified  
234 in this study. Similar to the A-BBOA observed in Tibetan Plateau, which has an O/C  
235 ratio of 0.51, this factor also has a relatively high O/C ratio of 0.48, greater than that of  
236 primary BBOA (O/C of 0.18–0.26)(Wang et al., 2017). These findings support that the  
237 second factor may be associated with the oxidation of biomass burning emissions. The  
238 temporal variation of ABBOA in the Tibetan Plateau was reported to be highly  
239 correlated with the potassium ion fraction ( $K^+$ ,  $r^2$  of 0.78), and  $K_3SO_4^+$  ( $r^2$  of 0.92).  
240 However, the temporal variation of the second factor in this study is only correlated  
241 well with that of  $K_3SO_4^+$  ( $r^2$  of 0.64) but not  $K^+$  ( $r^2$  of 0.01). The reason for this  
242 phenomenon is that the major source of  $K^+$  in remote sites like the Tibetan Plateau was  
243 long-distance transport of  $K_2SO_4$  particles, which probably from biomass burning-  
244 related K-containing salts interacts with  $H_2SO_4$  (Buxton et al., 1999). In contrast, there  
245 are multiple primary sources of  $K^+$  in  $PM_{10}$  (e.g., diesel-vehicle emissions, and mainly  
246 KCl particles) in urban areas (Figure S3). Based on these observations,  $K_3SO_4^+$  could  
247 be defined as an external A-BBOA indicator. Moreover, a previous transmission  
248 electron microscopy study also showed that significant agricultural BBOA was mixed  
249 with soot and transport from the North China Plain to urban Beijing, meanwhile,  $K_2SO_4$   
250 was also identified within those single BBOA-soot particles (Li et al., 2010). Hence,  
251 this second factor is identified as A-BBOA that was subjected to oxidation during  
252 transport to the measurement area as presented in the fire-point map and three-day back  
253 trajectories (Figure S4). June should be the month with maximum agricultural-related  
254 biomass burning in the North China Plain, although we thought that such burning  
255 activities had been banned in recent years (Shen et al., 2019).

256 The OOA1 factor has an O/C of 0.28 (Figure 2h). Similar to the NR- $PM_{10}$  LO-OOA  
257 (Xu et al., 2019b), it is highly correlated with  $C_2H_3O^+$  ( $r^2$  of 0.72). The  $C_2H_3O^+$  ion ( $m/z$   
258 = 43) is an important component of secondary organic aerosol (SOA)(Collier et al.,  
259 2015;Ng et al., 2011) and the diurnal patterns of the OOA1 and  $C_2H_3O^+$  both show a  
260 great enhancement around noontime (Figure S5), indicating the importance of  
261 secondary formation of less oxidized organic aerosol through daytime photochemical  
262 activity.

263           The OOA2 factor has an O/C of 0.42 (Figure 2i) and the OOA3 factor has a smaller  
264 O/C of 0.32 (Figure 2j). OOA2 correlated strongly with sulfate ( $r^2$  of 0.92; Figure 2d)  
265 and OOA3 correlated highly with nitrate ( $r^2$  of 0.97; Figure 2e). These features agree  
266 well with the **previous** observation for low-volatility OOA (sulfate-related OOA) and  
267 semi-volatile OOA (nitrate-related OOA) in Tibetan Plateau (Wang et al., 2017).

### 268 3.3. Comparison of NR-PM<sub>1</sub> and BC-PM<sub>1</sub> OA factors

269 The sum of the above-mentioned BC-PM<sub>1</sub> A-BBOA, OOA<sub>2</sub>, and OOA<sub>3</sub> fractions  
270 is comparable to the NR-PM<sub>1</sub> MO-OOA factor, based on their high O/C ratios. Figures  
271 3a-c are comparisons of the mass loadings of HOA, LO-OOA, and MO-OOA in both  
272 NR-PM<sub>1</sub> and BC-PM<sub>1</sub>. NR-PM<sub>1</sub> HOA, LO-OOA, and MO-OOA are strongly correlated  
273 with their counterpart fractions of BC-PM<sub>1</sub>, with  $r^2$  values of 0.68, 0.60, and 0.61,  
274 respectively. In Case I, most of the time, the mass loadings of BC-PM<sub>1</sub> HOA and MO-  
275 OOA are higher than those in NR-PM<sub>1</sub>, while LO-OOA shows the opposite trend. In  
276 Case II, the mass loadings of BC-PM<sub>1</sub> HOA are also generally higher than those of NR-  
277 PM<sub>1</sub> HOA, however, NR-PM<sub>1</sub> MO-OOA and LO-OOA are almost two folds higher than  
278 those of BC-PM<sub>1</sub>. Figures 3d-f are comparisons of the fractions of HOA, LO-OOA, and  
279 MO-OOA in NR-PM<sub>1</sub> and non-BC material in BC-PM<sub>1</sub> (coatings), respectively. In Case  
280 I, the fractions of HOA and MO-OOA internally-mixed with BC are almost two times  
281 and four times higher, respectively, than those in NR-PM<sub>1</sub>, whereas the two LO-OOA  
282 fractions closely track each other. In Case II, two LO-OOA fractions are still overlapped,  
283 but compared to Case I, the fraction of HOA in BC-PM<sub>1</sub> coatings is over four times that  
284 of NR-PM<sub>1</sub> HOA, and the difference between the two MO-OOA fractions is smaller.

285 As shown in Figure 4, the average of BC-PM<sub>1</sub> HOA fractions ( $0.27 \pm 0.17$  and  $0.11$   
286  $\pm 0.07$ , respectively) are higher than those in NR-PM<sub>1</sub> ( $0.12 \pm 0.08$  and  $0.02 \pm 0.02$ ,  
287 respectively) in both Case I and Case II, indicating that HOA particles is more internally  
288 mixed with BC compared to other OA materials. However, the possibility that RIE of  
289 OA coating may be lower than the default RIE value should also be considered.

290 The average mass loadings of NR-PM<sub>1</sub> LO-OOA in both Case I and Case II were  
291 higher than those of BC-PM<sub>1</sub>. However, the fraction of LO-OOA in both NR-PM<sub>1</sub> and  
292 BC-PM<sub>1</sub> coatings were very close to each other during the two cases, with an average  
293 value of  $0.23 \pm 0.10$  and  $0.25 \pm 0.12$ , respectively, indicating that the probability of LO-  
294 OOA condensation onto the two different types of particles is similar.

295 A greater difference between the MO-OOA fractions in NR-PM<sub>1</sub> and BC-PM<sub>1</sub> was  
296 observed in Case I than in Case II, and there is more MO-OOA in BC-PM<sub>1</sub> than in NR-  
297 PM<sub>1</sub> in Case I. A similar comparison between NR-PM<sub>1</sub> MO-OOA with BC-PM<sub>1</sub> MO-

298 OOA without A-BBOA can be found in SI (Figure S6), which shows closer fractions in  
299 both Case I and Case II. Therefore, one possibility that may cause higher MO-OOA  
300 fraction in BC-PM<sub>1</sub> than that in NR-PM<sub>1</sub> in Case I is the presence of the BC-PM<sub>1</sub> A-  
301 BBOA, which is only identified from the BC-PM<sub>1</sub> OA. More details of the BC-PM<sub>1</sub> A-  
302 BBOA are discussed in Section 3.4.

303

#### 304 **3.4. Characteristics of A-BBOA in BC-containing PM<sub>1</sub>**

305 Figure 5 shows the high-resolution mass spectra of A-BBOA observed in Nam Co  
306 (June 2015) and Beijing (June 2017) by laser-only SP-AMS. A mass spectra very  
307 similar to that observed in Beijing was also observed in Nanjing (February 2017)(Wu  
308 et al., 2019), with a  $r^2$  of 0.95. The A-BBOA observed in Nam Co (the Tibetan Plateau)  
309 was found in the thickest coated and internally-mixed BC-PM<sub>1</sub> (the mass ratio of  
310 coatings to BC core ( $R_{BC}$ ) can reach 14), which enhances the light absorption ability  
311 ( $E_{abs}$ ) of the BC core by a factor of 1.5 to 2.0 via the “lensing effect”.

312 As shown in Figure 6, A-BBOA was associated with those large particles ( $D_{va} >$   
313 300nm) which were also heavily-coated ( $R_{BC} > 9$ , Figure 6a and 6c). Because A-BBOA  
314 is a moderately aged OA, the OSc was very steady when  $R_{BC} > 9$  (Figure 6c). Figure  
315 6b presents the fractions of the OA factors (left) and the degree of light absorption  
316 enhancement ( $E_{abs}$ , estimated by the mass ratios of BC measured by Aethalometer  
317 model 33 and SP-AMS), as a function of  $R_{BC}$ . Figure 6d shows the temporal variations  
318 of the fractions of NR-PM<sub>1</sub> OA and BC-PM<sub>1</sub> OA from 15:00 to 24:00 on June 17, 2017  
319 when the highest A-BBOA concentrations were observed. There is a significant  
320 enhancement of A-BBOA which may account for up to 60% of the total OA coatings,  
321 which could enhance the BC-PM<sub>1</sub> MO-OOA fraction (within the purple frame in the  
322 bottom panel of Figure 6d).

323 In this study, A-BBOA was only observed by SP-AMS and was indeed only  
324 associated with BC. It is likely that A-BBOA was emitted together with BC when  
325 burning biomass fuel, and was oxidized subsequently during the transport. However,  
326 we cannot exclude the possibility that A-BBOA can be detected by HR-AMS. For  
327 example, it might be included in NR-PM<sub>1</sub> MO-OOA factor. Without separating A-

328 BBOA from other organic species, the source apportionment for HR-AMS may obscure  
329 air-quality- and climate-related implications of A-BBOA in the atmosphere, such as the  
330 enhancement of aerosol light absorption ability (Figure 6b).

#### 331 **4. Conclusions and implications**

332 Online chemical characteristics of BC and its associated species was for the first  
333 time elucidated in urban Beijing in summer, and compared with those of NR-PM<sub>1</sub>  
334 species. The biggest difference between the two measurements was in the composition  
335 of the organic species. In particular, we found BC in urban Beijing in June is partially  
336 of agricultural fire origin and, an unique biomass burning-related OA factor (A-BBOA)  
337 which was moderately aged, only existed in thickly coated BC-PM<sub>1</sub> ( $R_{BC} > 9$ ), but not  
338 NR-PM<sub>1</sub>. The unique A-BBOA could make up a significant portion of BC coating  
339 material. In addition to Beijing, similar A-BBOA was also identified in other locations,  
340 such as central Tibet Plateau (Wang et al., 2017) and Nanjing (Wu et al., 2019),  
341 suggesting that it may be ubiquitously present in BC-PM<sub>1</sub> in ambient atmosphere.

342 BBOA species are known to constitute a large portion of light-absorbing organics  
343 (brown carbon, BrC). The delay of BBOA oxidation and its longer duration time on BC  
344 cores can extend the impacts of BC. Moreover, together with our previous study of BC-  
345 associated A-BBOA in Tibet, results presented herein demonstrate that A-BBOA could  
346 lead to thick coating on BC cores, meaning a significant “lensing effect” to the  
347 enhancement of BC light absorption (Liu et al., 2017). As a key component of BC  
348 coating, presence of this factor may also alter the bulk hygroscopicity of BC-PM<sub>1</sub>. It  
349 could therefore affect its ability as cloud condensation nuclei (CCN)(Wu et al., 2019).  
350 Overall, the emission, evolution and transport of such A-BBOA, may influence the  
351 atmospheric behaviors and influence the role of BC in the air quality and climate (e.g.,  
352 radiative forcing and precipitation). We propose that future laboratory, field, and  
353 modeling studies are needed to verify the presence of A-BBOA, and to evaluate the  
354 regional environmental impacts of it.

355

*Data availability.* The data in this study are available from the authors upon request  
(caxinra@163.com).

*Supplement.* The supplement related to this article is available online at: xxx.

*Author contributions.* JF, DL, YW, JZ, WX, CX, FS and XG conducted the measurements and analyzed the data. JF, JY and PO wrote the first draft, JZ, PO, YQ, XZ, AL, SM, PF, DJ, QZ, YS, MC and XG contributed to the analyses and improvement of the paper. JF and XG contributed to the revision of the paper.

*Competing interests.* The authors declare that they have no conflict of interest.

*Special issue statement.* This article is part of the special issue “In-depth study of air pollution sources and processes within Beijing and its surrounding region (APHH-Beijing) (ACP/AMT inter-journal SI)”. It is not associated with a conference.

#### *Acknowledgements*

The authors from PRC acknowledge support from the National Natural Science Foundation of China (21777073) and the National Key Research and Development Program of China (No. 2018YFC0213802). The authors from Harvard and NUIST acknowledge additional support through the Harvard-NUIST Joint Laboratory for Air Quality and Climate (JLAQC).

#### **ABBREVIATIONS**

BC Black carbon

PM<sub>1</sub> Particulate matter with an aerodynamic diameter smaller than 1 μm

NR-PM<sub>1</sub> non-refractory PM<sub>1</sub>

BC-PM<sub>1</sub> BC-containing particles in PM<sub>1</sub>

BrC Brown carbon

HR-AMS High-resolution aerosol mass spectrometer (Aerodyne Research Inc.)

SP-AMS Soot-particle aerosol mass spectrometer (Aerodyne Research Inc.)

IE Ionization efficiency

RIE Relative ionization efficiency

HRMS High-resolution mass spectra

PMF Positive matrix factorization



OA Organic aerosol

SOA Secondary organic aerosol O/C Oxygen-to-carbon ratio

H/C Hydrogen-to-carbon ratio

A-BBOA Aged biomass burning organic aerosol

SV-OOA Semi-volatile oxygenated organic aerosol

LV-OOA low-volatility oxygenated organic aerosol

MO-OOA more-oxidized oxygenated organic aerosol

LO-OOA less-oxidized oxygenated organic aerosol

$R_{BC}$  mass ratio of BC coatings to BC

$D_{va}$  Vacuum aerodynamic diameter

## References

- 356 Bond, T. C., Doherty, S. J., Fahey, D. W., Forster, P. M., Bernsten, T., DeAngelo, B. J., Flanner, M.  
357 G., Ghan, S., Kärcher, B., Koch, D., Kinne, S., Kondo, Y., Quinn, P. K., Sarofim, M. C., Schultz, M.  
358 G., Schulz, M., Venkataraman, C., Zhang, H., Zhang, S., Bellouin, N., Guttikunda, S. K., Hopke, P.  
359 K., Jacobson, M. Z., Kaiser, J. W., Klimont, Z., Lohmann, U., Schwarz, J. P., Shindell, D., Storelvmo,  
360 T., Warren, S. G., and Zender, C. S.: Bounding the role of black carbon in the climate system: A  
361 scientific assessment, *J. Geophys. Res.- Atmos.*, 118, 5380-5552, 10.1002/jgrd.50171, 2013.
- 362 Buseck, P. R., Adachi, K., Gelencsér, A., Tompa, É., and Pósfai, M.: Ns-Soot: A Material-Based  
363 Term for Strongly Light-Absorbing Carbonaceous Particles, *Aerosol Sci. Technol.*, 48, 777-788,  
364 10.1080/02786826.2014.919374, 2014.
- 365 Canagaratna, M. R., Jayne, J. T., Jimenez, J. L., Allan, J. D., Alfarra, M. R., Zhang, Q., Onasch, T.  
366 B., Drewnick, F., Coe, H., Middlebrook, A., Delia, A., Williams, L. R., Trimborn, A. M., Northway,  
367 M. J., DeCarlo, P. F., Kolb, C. E., Davidovits, P., and Worsnop, D. R.: Chemical and microphysical  
368 characterization of ambient aerosols with the aerodyne aerosol mass spectrometer, *Mass Spectrom.*  
369 *Rev.*, 26, 185-222, 10.1002/Mas.20115, 2007.
- 370 Canagaratna, M. R., Jimenez, J. L., Kroll, J. H., Chen, Q., Kessler, S. H., Massoli, P., Hildebrandt  
371 Ruiz, L., Fortner, E., Williams, L. R., Wilson, K. R., Surratt, J. D., Donahue, N. M., Jayne, J. T., and  
372 Worsnop, D. R.: Elemental ratio measurements of organic compounds using aerosol mass  
373 spectrometry: characterization, improved calibration, and implications, *Atmos. Chem. Phys.*, 15,  
374 253-272, 10.5194/acp-15-253-2015, 2015a.
- 375 Canagaratna, M. R., Massoli, P., Browne, E. C., Franklin, J. P., Wilson, K. R., Onasch, T. B.,  
376 Kirchstetter, T. W., Fortner, E. C., Kolb, C. E., Jayne, J. T., Kroll, J. H., and Worsnop, D. R.:  
377 Chemical Compositions of Black Carbon Particle Cores and Coatings via Soot Particle Aerosol  
378 Mass Spectrometry with Photoionization and Electron Ionization, *J. Phys. Chem. A*, 119, 4589-4599,  
379 10.1021/jp510711u, 2015b.
- 380 Cappa, C. D., Onasch, T. B., Massoli, P., Worsnop, D. R., Bates, T. S., Cross, E. S., Davidovits, P.,  
381 Hakala, J., Hayden, K. L., Jobson, B. T., Kolesar, K. R., Lack, D. A., Lerner, B. M., Li, S.-M.,  
382 Mellon, D., Nuaaman, I., Olfert, J. S., Petäjä, T., Quinn, P. K., Song, C., Subramanian, R., Williams,  
383 E. J., and Zaveri, R. A.: Radiative absorption enhancements due to the mixing state of atmospheric  
384 black carbon, *Science*, 337, 1078-1081, 10.1126/science.1223447, 2012.
- 385 Chen, B., Andersson, A., Lee, M., Kirillova, E. N., Xiao, Q., Kruså, M., Shi, M., Hu, K., Lu, Z.,  
386 Streets, D. G., Du, K., and Gustafsson, Ö.: Source Forensics of Black Carbon Aerosols from China,  
387 *Environ. Sci. Technol.*, 47, 9102-9108, 10.1021/es401599r, 2013.
- 388 Chen, Y.; Cai, J.; Wang, Z.; Peng, C.; Yao, X.; Tian, M.; Han, Y.; Shi, G.; Shi, Z.; Liu, Y.; Yang, X.;  
389 Zheng, M.; Zhu, T.; He, K.; Zhang, Q.; Yang, F. Simultaneous measurements of urban and rural  
390 particles in Beijing – Part 1: Chemical composition and mixing state. *Atmos. Chem. Phys.*, 20, 9231-  
391 9247, 10.5194/acp-20-9231-2020, 2020a.
- 392 Chen, Y.; Shi, G.; Cai, J.; Shi, Z.; Wang, Z.; Yao, X.; Tian, M.; Peng, C.; Han, Y.; Zhu, T.; Liu, Y.;  
393 Yang, X.; Zheng, M.; Yang, F.; Zhang, Q.; He, K. Simultaneous measurements of urban and rural  
394 particles in Beijing – Part 2: Case studies of haze events and regional transport. *Atmos. Chem. Phys.*,  
395 20, 9249-9263, 10.5194/acp-20-9249-2020, 2020b.
- 396 China, S., Scarnato, B., Owen, R. C., Zhang, B., Ampadu, M. T., Kumar, S., Dzepina, K., Dziobak,  
397 M. P., Fialho, P., Perlinger, J. A., Hueber, J., Helmig, D., Mazzoleni, L. R., and Mazzoleni, C.:  
398 Morphology and mixing state of aged soot particles at a remote marine free troposphere site:

399 Implications for optical properties, *Geophys. Res. Lett.*, 42, 1243-1250, 10.1002/2014gl062404,  
400 2015.

401 Collier, S., Zhou, S., Kuwayama, T., Forestieri, S., Brady, J., Zhang, M., Kleeman, M., Cappa, C.,  
402 Bertram, T., and Zhang, Q.: Organic PM Emissions from Vehicles: Composition, O/C Ratio, and  
403 Dependence on PM Concentration, *Aerosol Sci. Technol.*, 49, 86-97,  
404 10.1080/02786826.2014.1003364, 2015.

405 Ge, X., Zhang, Q., Sun, Y., Ruehl, C. R., and Setyan, A.: Effect of aqueous-phase processing on  
406 aerosol chemistry and size distributions in Fresno, California, during wintertime, *Environ. Chem.*,  
407 9, 221-235, <http://dx.doi.org/10.1071/EN11168>, 2012a.

408 Ge, X. L., Setyan, A., Sun, Y., and Zhang, Q.: Primary and secondary organic aerosols in Fresno,  
409 California during wintertime: Results from high resolution aerosol mass spectrometry, *J. Geophys.*  
410 *Res.- Atmos.*, 117, D19301, 10.1029/2012jd018026, 2012b.

411 Janssen, N.A.H., Gerlofs-Nijland, M., Lanki, T., Salonen, R.O., Cassee, F., Hoek, G., Fischer, P.,  
412 Brunekreef, B., Krzyzanowski, M, Health effects of black carbon, WHO, 2012.  
413 [https://www.euro.who.int/\\_data/assets/pdf\\_file/0004/162535/e96541.pdf?ua=1](https://www.euro.who.int/_data/assets/pdf_file/0004/162535/e96541.pdf?ua=1)

414 Lee, A. K. Y., Chen, C. L., Liu, J., Price, D. J., Betha, R., Russell, L. M., Zhang, X., and Cappa, C.  
415 D.: Formation of secondary organic aerosol coating on black carbon particles near vehicular  
416 emissions, *Atmos. Chem. Phys.*, 17, 15055-15067, 10.5194/acp-17-15055-2017, 2017.

417 Lee, B. P., Li, Y. J., Yu, J. Z., Louie, P. K. K., and Chan, C. K.: Physical and chemical  
418 characterization of ambient aerosol by HR-ToF-AMS at a suburban site in Hong Kong during  
419 springtime 2011, *Journal of Geophysical Research: Atmospheres*, n/a-n/a, 10.1002/jgrd.50658, 2013.

420 Li, W. J., Shao, L. Y., and Buseck, P. R.: Haze types in Beijing and the influence of agricultural  
421 biomass burning, *Atmos. Chem. Phys.*, 10, 8119-8130, 10.5194/acp-10-8119-2010, 2010.

422 Li, Y. J., Lee, B. P., Su, L., Fung, J. C. H., and Chan, C. K.: Seasonal characteristics of fine  
423 particulate matter (PM) based on high-resolution time-of-flight aerosol mass spectrometric (HR-  
424 ToF-AMS) measurements at the HKUST Supersite in Hong Kong, *Atmos. Chem. Phys.*, 15, 37-53,  
425 10.5194/acp-15-37-2015, 2015.

426 Liu, C., Chung, C. E., Yin, Y., and Schnaiter, M.: The absorption Ångström exponent of black carbon:  
427 from numerical aspects, *Atmos. Chem. Phys.*, 18, 6259-6273, 10.5194/acp-18-6259-2018, 2018.

428 Liu, D., Whitehead, J., Alfarra, M. R., Reyes-Villegas, E., Spracklen, Dominick V., Reddington,  
429 Carly L., Kong, S., Williams, Paul I., Ting, Y.-C., Haslett, S., Taylor, Jonathan W., Flynn, Michael J.,  
430 Morgan, William T., McFiggans, G., Coe, H., and Allan, James D.: Black-carbon absorption  
431 enhancement in the atmosphere determined by particle mixing state, *Nature Geosci.*, 10, 184-188,  
432 10.1038/ngeo2901, 2017.

433 Liu, D., Joshi, R., Wang, J., Yu, C., Allan, J. D., Coe, H., Flynn, M. J., Xie, C., Lee, J., and Squires,  
434 F.: Contrasting physical properties of black carbon in urban Beijing between winter and summer,  
435 *Atmos. Chem. Phys.*, 6749-6769, 2019.

436 Massoli, P., Onasch, T. B., Cappa, C. D., Nuamaan, I., Hakala, J., Hayden, K., Li, S.-M., Sueper, D.  
437 T., Bates, T. S., Quinn, P. K., Jayne, J. T., and Worsnop, D. R.: Characterization of black carbon-  
438 containing particles from soot particle aerosol mass spectrometer measurements on the R/V Atlantis  
439 during CalNex 2010, *J. Geophys. Res.- Atmos.*, 120, 2014JD022834, 2015.

440 Ng, N. L., Canagaratna, M. R., Jimenez, J. L., Chhabra, P. S., Seinfeld, J. H., and Worsnop, D. R.:  
441 Changes in organic aerosol composition with aging inferred from aerosol mass spectra, *Atmos.*  
442 *Chem. Phys.*, 11, 6465-6474, 10.5194/acp-11-6465-2011, 2011.

443 Onasch, T. B., Trimborn, A., Fortner, E. C., Jayne, J. T., Kok, G. L., Williams, L. R., Davidovits, P.,  
444 and Worsnop, D. R.: Soot Particle Aerosol Mass Spectrometer: Development, Validation, and Initial  
445 Application, *Aerosol Science and Technology*, 46, 804-817, 10.1080/02786826.2012.663948, 2012.  
446 Paatero, P., and Tapper, U.: Positive matrix factorization: A non-negative factor model with optimal  
447 utilization of error estimates of data values, *Environmetrics*, 5, 111-126, 10.1002/env.3170050203,  
448 1994.

449 Qiu, Y., Xie, Q., Wang, J., Xu, W., Li, L., Wang, Q., Zhao, J., Chen, Y., Chen, Y., Wu, Y., Du, W.,  
450 Zhou, W., Lee, J., Zhao, C., Ge, X., Fu, P., Wang, Z., Worsnop, D. R., and Sun, Y.: Vertical  
451 Characterization and Source Apportionment of Water-Soluble Organic Aerosol with High-  
452 resolution Aerosol Mass Spectrometry in Beijing, China, *ACS Earth Space Chem.*, 3, 273-284,  
453 10.1021/acsearthspacechem.8b00155, 2019.

454 Ramanathan, V., and Carmichael, G.: Global and regional climate changes due to black carbon,  
455 *Nature Geosci*, 1, 221-227, 2008.

456 Saleh, R., Marks, M., Heo, J., Adams, P. J., Donahue, N. M., and Robinson, A. L.: Contribution of  
457 brown carbon and lensing to the direct radiative effect of carbonaceous aerosols from biomass and  
458 biofuel burning emissions, *J. Geophys. Res.- Atmos.*, 120, 10,285-210,296, 10.1002/2015jd023697,  
459 2015.

460 Shen, L., Jacob, D. J., Zhu, L., Zhang, Q., Zheng, B., Sulprizio, M. P., Li, K., De Smedt, I., González  
461 Abad, G., Cao, H., Fu, T.-M., and Liao, H.: The 2005–2016 Trends of Formaldehyde Columns Over  
462 China Observed by Satellites: Increasing Anthropogenic Emissions of Volatile Organic Compounds  
463 and Decreasing Agricultural Fire Emissions, *Geophys. Res. Lett.*, 46, 4468-4475,  
464 10.1029/2019gl082172, 2019.

465 Shi, Z., Vu, T., Kotthaus, S., Harrison, R. M., Grimmond, S., Yue, S., Zhu, T., Lee, J., Han, Y.,  
466 Demuzere, M., Dunmore, R. E., Ren, L., Liu, D., Wang, Y., Wild, O., Allan, J., Acton, W. J., Barlow,  
467 J., Barratt, B., Beddows, D., Bloss, W. J., Calzolari, G., Carruthers, D., Carslaw, D. C., Chan, Q.,  
468 Chatzidiakou, L., Chen, Y., Crilley, L., Coe, H., Dai, T., Doherty, R., Duan, F., Fu, P., Ge, B., Ge,  
469 M., Guan, D., Hamilton, J. F., He, K., Heal, M., Heard, D., Hewitt, C. N., Hollaway, M., Hu, M., Ji,  
470 D., Jiang, X., Jones, R., Kalberer, M., Kelly, F. J., Kramer, L., Langford, B., Lin, C., Lewis, A. C.,  
471 Li, J., Li, W., Liu, H., Liu, J., Loh, M., Lu, K., Lucarelli, F., Mann, G., McFiggans, G., Miller, M.  
472 R., Mills, G., Monk, P., Nemitz, E., O'Connor, F., Ouyang, B., Palmer, P. I., Percival, C., Popoola,  
473 O., Reeves, C., Rickard, A. R., Shao, L., Shi, G., Spracklen, D., Stevenson, D., Sun, Y., Sun, Z., Tao,  
474 S., Tong, S., Wang, Q., Wang, W., Wang, X., Wang, X., Wang, Z., Wei, L., Whalley, L., Wu, X., Wu,  
475 Z., Xie, P., Yang, F., Zhang, Q., Zhang, Y., Zhang, Y., and Zheng, M.: Introduction to the special  
476 issue “In-depth study of air pollution sources and processes within Beijing and its surrounding  
477 region (APHH-Beijing)”, *Atmos. Chem. Phys.*, 19, 7519-7546, 10.5194/acp-19-7519-2019, 2019.

478 Sun, Y., Jiang, Q., Wang, Z., Fu, P., Li, J., Yang, T., and Yin, Y.: Investigation of the Sources and  
479 Evolution Processes of Severe Haze Pollution in Beijing in January 2013, *J. Geophys. Res.- Atmos.*,  
480 2014JD021641, 10.1002/2014JD021641, 2014.

481 Sun, Y., Jiang, Q., Xu, Y., Ma, Y., Zhang, Y., Liu, X., Li, W., Wang, F., Li, J., Wang, P., and Li, Z.:  
482 Aerosol characterization over the North China Plain: Haze life cycle and biomass burning impacts  
483 in summer, *J. Geophys. Res.- Atmos.*, 121, 2508-2521, 10.1002/2015jd024261, 2016.

484 Sun, Y. L., Zhang, Q., Schwab, J. J., Chen, W. N., Bae, M. S., Hung, H. M., Lin, Y. C., Ng, N. L.,  
485 Jayne, J., Massoli, P., Williams, L. R., and Demerjian, K. L.: Characterization of near-highway  
486 submicron aerosols in New York City with a high-resolution aerosol mass spectrometer, *Atmos.*

487 Chem. Phys., 12, 2215-2227, 10.5194/acp-12-2215-2012, 2012.

488 Ulbrich, I. M., Canagaratna, M. R., Zhang, Q., Worsnop, D. R., and Jimenez, J. L.: Interpretation of  
489 organic components from Positive Matrix Factorization of aerosol mass spectrometric data, Atmos.  
490 Chem. Phys., 9, 2891-2918, 10.5194/acp-9-2891-2009, 2009.

491 V. Buxton, G., Bydder, M., and Arthur Salmon, G.: The reactivity of chlorine atoms in aqueous  
492 solution. Part II. The equilibrium  $\text{SO}_4^- + \text{Cl}^- \text{Cl}^{\text{Nsb}} + \text{SO}_4^{2-}$ , Phys. Chem. Chem. Phys., 1, 269-273,  
493 10.1039/A807808D, 1999.

494 Wang, J., Onasch, T. B., Ge, X., Collier, S., Zhang, Q., Sun, Y., Yu, H., Chen, M., Prévôt, A. S., and  
495 Worsnop, D. R.: Observation of fullerene soot in eastern China, Environ. Sci. Technol. Lett., 3, 121-  
496 126, 10.1021/acs.estlett.6b00044, 2016.

497 Wang, J., Zhang, Q., Chen, M., Collier, S., Zhou, S., Ge, X., Xu, J., Shi, J., Xie, C., and Hu, J.: First  
498 chemical characterization of refractory black carbon aerosols and associated coatings over the  
499 Tibetan Plateau (4730 m asl), Environ. Sci. Technol., 51, 14072-14082, 10.1021/acs.est.7b03973,  
500 2017.

501 Wang, J., Liu, D., Ge, X., Wu, Y., Shen, F., Chen, M., Zhao, J., Xie, C., Wang, Q., and Xu, W.:  
502 Characterization of black carbon-containing fine particles in Beijing during wintertime, Atmos.  
503 Chem. Phys., 19, 447-458, 10.5194/acp-19-447-2019, 2019.

504 Willis, M. D., Lee, A. K. Y., Onasch, T. B., Fortner, E. C., Williams, L. R., Lambe, A. T., Worsnop,  
505 D. R., and Abbatt, J. P. D.: Collection efficiency of the soot-particle aerosol mass spectrometer (SP-  
506 AMS) for internally mixed particulate black carbon, Atmos. Meas. Tech., 7, 4507-4516,  
507 10.5194/amt-7-4507-2014, 2014.

508 Wu, Y., Liu, D., Wang, J., Shen, F., Chen, Y., Cui, S., Ge, S., Wu, Y., Chen, M., and Ge, X.:  
509 Characterization of Size-Resolved Hygroscopicity of Black Carbon-Containing Particle in Urban  
510 Environment, Environ. Sci. Technol., 53, 14212-14221, 10.1021/acs.est.9b05546, 2019.

511 Xie, C., Xu, W., Wang, J., Liu, D., Ge, X., Zhang, Q., Wang, Q., Du, W., Zhao, J., Zhou, W., Li, J.,  
512 Fu, P., Wang, Z., Worsnop, D., and Sun, Y.: Light absorption enhancement of black carbon in urban  
513 Beijing in summer, Atmos. Environ., 213, 499-504, 10.1016/j.atmosenv.2019.06.041, 2019a.

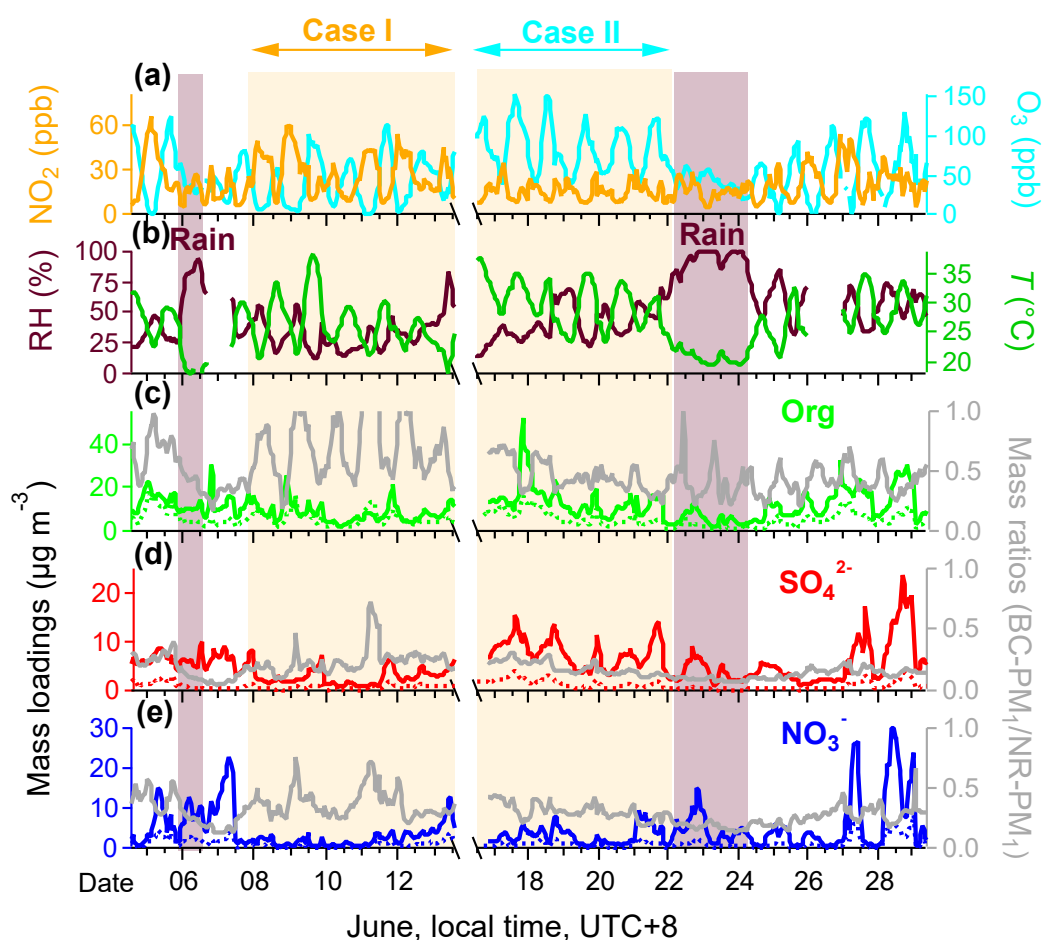
514 Xie, C., Xu, W., Wang, J., Wang, Q., Liu, D., Tang, G., Chen, P., Du, W., Zhao, J., and Zhang, Y.:  
515 Vertical characterization of aerosol optical properties and brown carbon in winter in urban Beijing,  
516 China, Atmos. Chem. Phys., 19, 165-179, 10.5194/acp-19-165-2019, 2019b.

517 Xu, J., Zhang, Q., Shi, J., Ge, X., Xie, C., Wang, J., Kang, S., Zhang, R., and Wang, Y.: Chemical  
518 characteristics of submicron particles at the central Tibetan Plateau: insights from aerosol mass  
519 spectrometry, Atmos. Chem. Phys., 18, 427-443, 10.5194/acp-18-427-2018, 2018.

520 Xu, W., Sun, Y., Wang, Q., Zhao, J., Wang, J., Ge, X., Xie, C., Zhou, W., Du, W., and Li, J.: Changes  
521 in aerosol chemistry from 2014 to 2016 in winter in Beijing: Insights from high-resolution aerosol  
522 mass spectrometry, J. Geophys. Res.- Atmos., 124, 1132-1147, 10.1029/2018JD029245, 2019a.

523 Xu, W., Xie, C., Karnezi, E., Zhang, Q., Wang, J., Pandis, S. N., Ge, X., Zhang, J., An, J., and Wang,  
524 Q.: Summertime aerosol volatility measurements in Beijing, China, Atmos Chem Phys, 19, 10205-  
525 10216, 10.5194/acp-19-10205-2019, 2019b.

526 Zhang, Q., Jimenez, J., Canagaratna, M., Ulbrich, I., Ng, N., Worsnop, D., and Sun, Y.:  
527 Understanding atmospheric organic aerosols via factor analysis of aerosol mass spectrometry: a  
528 review, Anal. Bioanal. Chem., 401, 3045-3067, 10.1007/s00216-011-5355-y, 2011.



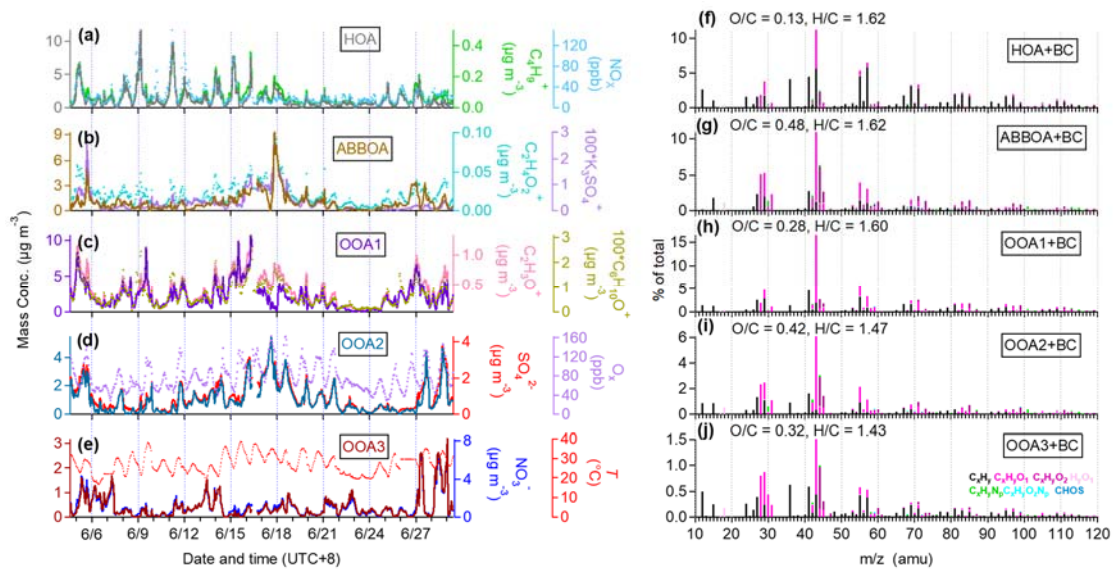
530

531 **Figure 1.** Temporal variations of selected chemical species measured in Beijing on June 4 -29, 2017.532 (a) mixing ratios of nitrogen dioxide ( $\text{NO}_2$ ) and ozone ( $\text{O}_3$ ); (b) 15-m relative humidity ( $RH$ ) and533 temperature ( $T$ ); (c-e) on the left are the mass loadings of organic (Org), sulfate ( $\text{SO}_4^{2-}$ ) and nitrate534 ( $\text{NO}_3^-$ ) measured by HR-AMS and SP-AMS, and on the right are mass ratios of individual BC-PM<sub>1</sub>535 species to NR-PM<sub>1</sub> species (e.g., BC-PM<sub>1</sub> Org to NR-PM<sub>1</sub> Org). The NR-PM<sub>1</sub> species measured by536 HR-AMS is in solid line, and the BC-PM<sub>1</sub> species measured by SP-AMS is in the dotted line. The

537 shaded areas are raining periods. The observation period is divided into two cases according to the

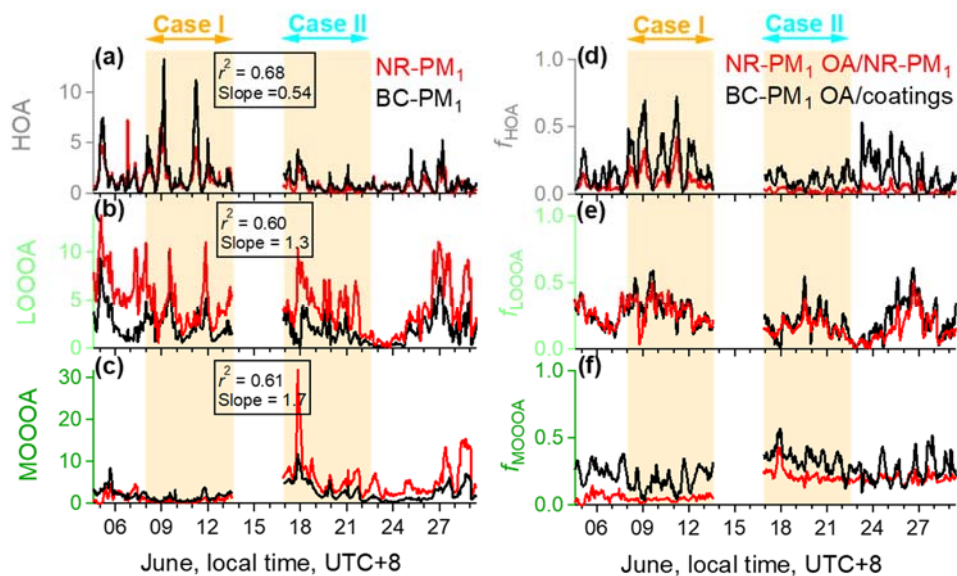
538 mixing ratio of nitrogen  $\text{NO}_2$ , Case I and Case II, which represent high  $\text{NO}_2$  and low  $\text{NO}_2$  mixing

539 ratios, respectively.



540

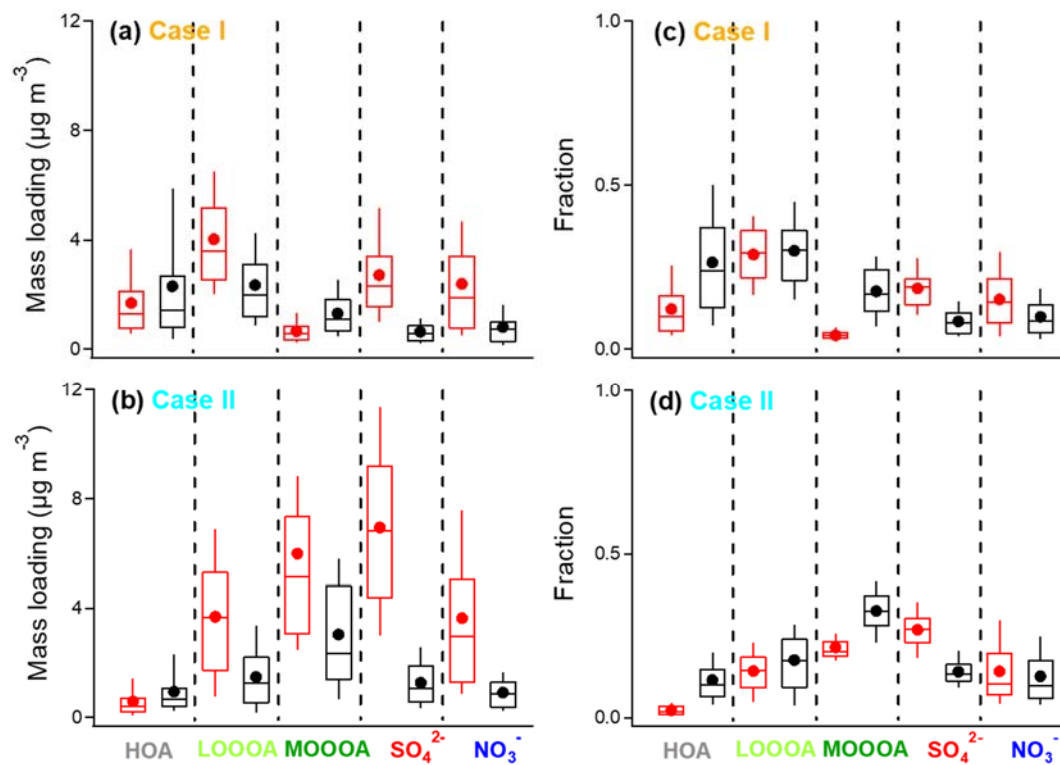
541 **Figure 2.** Temporal variations (left panels), high-resolution mass spectra (right panels) of five OA  
 542 factors in summer 2017: (a) and (f) HOA, (b) and (g) A-BBOA, (c) and (h) OOA1 (LO-OOA), (d)  
 543 and (i) OOA2, and (e) and (j) OOA3. Also shown in the left panels are the time series of other  
 544 tracers, including  $C_4H_9^+$ ,  $NO_x$ ,  $C_2H_4O_2^+$ ,  $K_3SO_4^+$ ,  $C_6H_{10}O^+$ ,  $C_2H_3O^+$ ,  $SO_4^{2-}$  and  $NO_3^-$ .



545

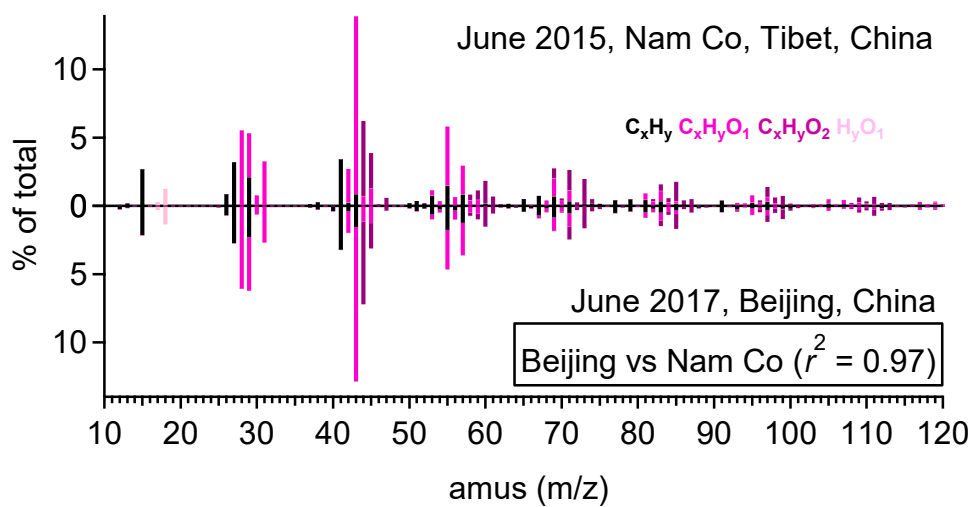
546 **Figure 3.** Temporal variations of NR-PM<sub>1</sub> and BC-PM<sub>1</sub> (a-c) HOA, LO-OOA, and MO-OOA (left  
 547 panels) and (d-e) their fractions. NR-PM<sub>1</sub> OA factors are in red, and the BC-PM<sub>1</sub> OA factors are in  
 548 black. Here BC-PM<sub>1</sub> MO-OOA is the sum of A-BBOA, OOA2 (sulfate-related OOA), and OOA3  
 549 (nitrate-related OOA).





550

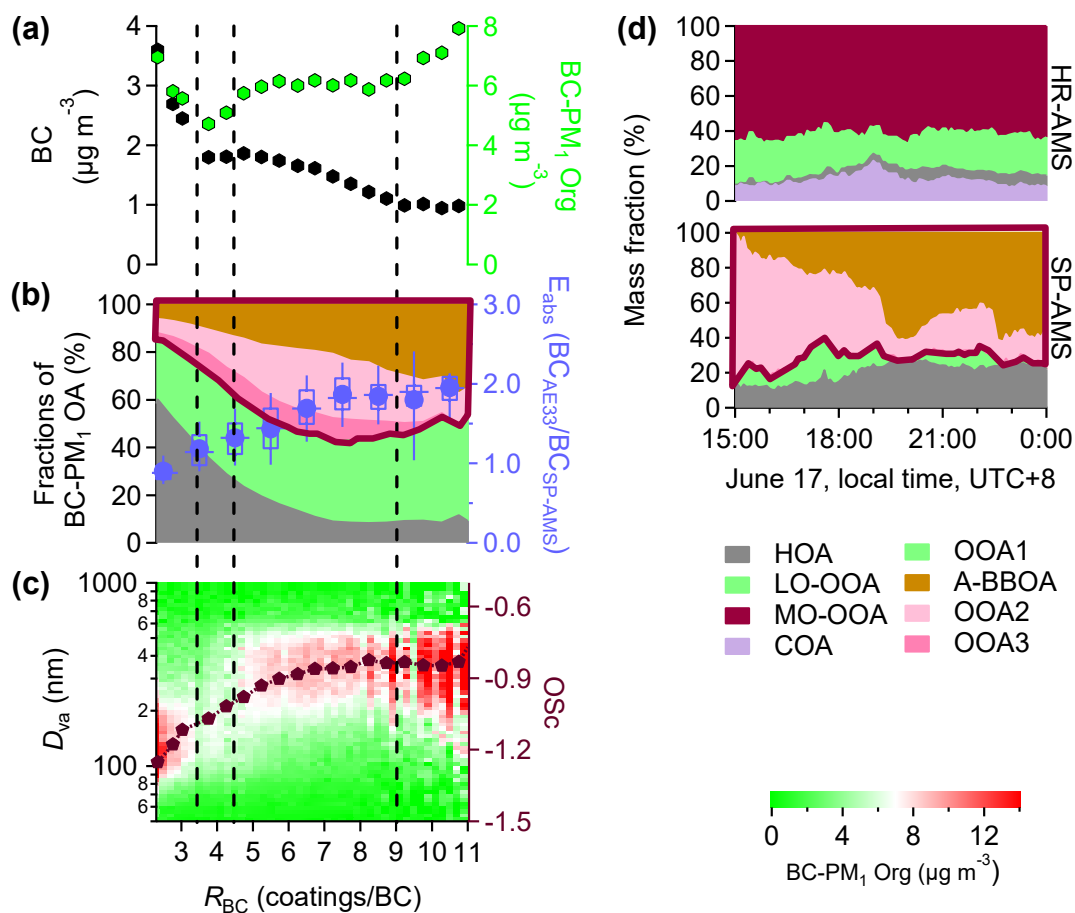
551 **Figure 4.** Box plots of mass loadings and fractions of five selected species (HOA, LO-OOA, MO-  
 552 OOA,  $\text{SO}_4^{2-}$ , and  $\text{NO}_3^-$ ) in Case I and Case II. The bounds of boxes represent quartiles, the whiskers  
 553 indicate the 90th and 10th percentiles, and the lines and dots inside the boxes are median and mean  
 554 values. NR-PM<sub>1</sub> OA factors are in red, and the BC-PM<sub>1</sub> OA factors are in black.



555

556 **Figure 5** Comparison between the high-resolution mass spectra of A-BBOA obtained in Nam Co

557 (June 2015) and Beijing (June 2017) (nitrogen-containing ions are not shown here).



558

559 **Figure 6.** (a-c) the mass loadings of BC, BC-PM<sub>1</sub> Org, fractions of BC-PM<sub>1</sub> OA factors,  $E_{\text{abs}}$ , the  
 560 oxidation state ( $\text{OSc} = 2 \cdot (\text{O}/\text{C}) - (\text{H}/\text{C})$ ) of BC-PM<sub>1</sub> Org, and the size distribution of BC-PM<sub>1</sub> Org  
 561 as a function of coating thickness ( $R_{\text{BC}}$ ). (d) temporal variations of OA fractions of NR-PM<sub>1</sub> and  
 562 BC-PM<sub>1</sub> from 15:00 to 24:00 on June 17, 2017.

563

564